Delft University of Technology

Low power wide spectrum optical transmitter using avalanche mode LEDs in SOI CMOS technology

Agarwal, V.; Dutta, S.; Annema, A.J.; Hueting, R.J.E.; Steeneken, Peter; Nauta, B.

DOI
10.1364/OE.25.016981

Publication date
2017

Document Version
Final published version

Published in
Optics Express

Citation (APA)
Agarwal, V., Dutta, S., Annema, A. J., Hueting, R. J. E., Steeneken, P., & Nauta, B. (2017). Low power wide spectrum optical transmitter using avalanche mode LEDs in SOI CMOS technology. *Optics Express*, *25*(15), 16981-16995. https://doi.org/10.1364/OE.25.016981

Important note
To cite this publication, please use the final published version (if applicable).
Please check the document version above.

Copyright
Other than for strictly personal use, it is not permitted to download, forward or distribute the text or part of it, without the consent of the author(s) and/or copyright holder(s), unless the work is under an open content license such as Creative Commons.

Takedown policy
Please contact us and provide details if you believe this document breaches copyrights.
We will remove access to the work immediately and investigate your claim.

This work is downloaded from Delft University of Technology.
For technical reasons the number of authors shown on this cover page is limited to a maximum of 10.

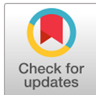

Research Article | Vol. 25, No. 15 | 24 Jul 2017 | OPTICS EXPRESS 16981

Optics EXPRESS

Low power wide spectrum optical transmitter using avalanche mode LEDs in SOI CMOS technology

VISHAL AGARWAL,[1,*] SATADAL DUTTA,[2] ANNE-JOHAN ANNEMA,[1] RAYMOND J. E. HUETING,[2] PETER G. STEENEKEN,[3] AND BRAM NAUTA[1]

[1] *Integrated Circuit Design, CTIT, University of Twente, 7500 AE, Enschede, The Netherlands*
[2] *Semiconductor Components, MESA+ Institute for Nanotechnology, University of Twente, 7500 AE, Enschede, The Netherlands*
[3] *Delft University of Technology, The Netherlands*
[*] *v.agarwal@utwente.nl*

Abstract: This paper presents a low power monolithically integrated optical transmitter with avalanche mode light emitting diodes in a 140 nm silicon-on-insulator CMOS technology. Avalanche mode LEDs in silicon exhibit wide-spectrum electroluminescence (400 nm $< \lambda <$ 850 nm), which has a significant overlap with the responsivity of silicon photodiodes. This enables monolithic CMOS integration of optocouplers, for e.g. smart power applications requiring high data rate communication with a large galvanic isolation. To ensure a certain minimum number of photons per data pulse (or per bit), light emitting diode drivers must be robust against process, operating conditions and temperature variations of the light emitting diode. Combined with the avalanche mode light emitting diode's steep current-voltage curve at relatively high breakdown voltages, this conventionally results in high power consumption and significant heating. The presented transmitter circuit is intrinsically robust against these issues, thereby enabling low power operation.

© 2017 Optical Society of America

OCIS codes: (250.3140) Integrated optoelectronic circuits; (130.3120) Integrated optics devices; (230.3670) Light-emitting diodes; (130.0250) Optoelectronics.

References and links

1. K. Gingerich and C. Sterzik, "The ISO72x Family of High-Speed Digital Isolators," Texas Instruments Inc., Application Report SLLA198 (2006).
2. D. A. B. Miller, "Device requirements for optical interconnects to silicon chips," Proc. IEEE **97**(7), 1166–1185 (2009).
3. R. Newman, "Visible light from a silicon p-n junction," Phys. Rev. **100**(2), 700–703 (1955).
4. M. du Plessis, H. Aharoni, and L.W. Snyman, "Silicon LEDs fabricated in standard VLSI technology as components for all silicon monolithic integrated optoelectronic systems," IEEE J. Sel. Topics Quantum Electron. **8**(6), 1412–1419 (2002).
5. S. Dutta, R.J.E. Hueting, A.J. Annema, L. Qi, L.K. Nanver and J. Schmitz, "Opto-electronic modeling of light emission from avalanche-mode silicon p^+n junctions," J. Appl. Phys. **118**(11), 114506 (2015).
6. A. Chatterjee, B. Bhuva, and R. Schrimpf, "High-speed light Modulation in avalanche breakdown mode for Si diodes," IEEE Electron Device Lett. **25**(9), 628–630 (2004).
7. B.P. van Drieënhuizen and R.F. Wolffenbuttel, "Optocoupler based on the avalanche light emission in silicon," Sensors Actuat. A: Physical **31**(1), 229–240 (1992).
8. L.W. Snyman, H. Aharoni, A. Biber, A. Bogalecki, L. Canning, M. du Plessis and P. Maree, "Optical sources, integrated optical detectors, and optical waveguides in standard silicon CMOS integrated circuitry," Proc. SPIE **3953**, 20–36 (2000).
9. B. Huang, X. Zhang, W. Wang, Z. Dong, N. Guan, Z. Zhang, and H. Chen, "CMOS monolithic optoelectronic integrated circuit for on-chip optical interconnection," Opt. Commun. **284**, 3924–3927 (2011).
10. S. Dutta, R.J.E. Hueting, V. Agarwal and A.J. Annema, "An integrated optical link in 140 nm SOI technology," in *Proc. Conference on Lasers and Electro-Optics, Session JW2A* (2016), paper 132.
11. S. Dutta, V. Agarwal, R.J.E. Hueting, J. Schmitz and A.J. Annema, "Monolithic optical link in silicon-on-insulator CMOS technology," Opt. Express **25**(5), 5440–5456 (2017).

#292795 https://doi.org/10.1364/OE.25.016981
Journal © 2017 Received 17 Apr 2017; revised 22 May 2017; accepted 22 May 2017; published 10 Jul 2017

12. Y. Wang, D. Luo, Q. Pan, L. Jing, Z. Li, and C. P. Yue, "A 60-GHz 4-Gb/s Fully Integrated NRZ-to-QPSK Fiber-Wireless Modulator," IEEE Trans. Circuits Syst. I, Reg. Papers **64**(3), 653–663 (2017).
13. P. Wessels, M. Swanenberg, H. van Zwol, B. Krabbenborg, H. Boezen, M. Berkhout, and A. Grakist, "Advanced BCD technology for automotive, audio and power applications," Solid-State Electronics **51**(2), 195–211 (2007).
14. A.G. Chynoweth and K.G. McKay, "Photon emission from Avalanche Breakdown in Silicon," Phys. Rev. **102**(2), 369–376 (1956).
15. E.F. Schubert, *Light-Emitting Diodes* (Cambridge University Press, 2006).
16. C. Kurtsiefer, P. Zarda, S. Mayer and H. Weinfurter, "The breakdown flash of Silicon Avalance Photodiodes – backdoor for eavesdropper attacks?" J. Mod. Opt. **48**(13), 2039–2047 (2001).
17. A. G. Stern, "Design of High Quantum Efficiency and High Resolution, Si/SiGe Avalanche Photodiode Focal Plane Arrays Using Novel, BackIlluminated, Silicon-on-Sapphire Substrates," in *Photodiodes-World Activities in 2011*, J. W. Park, (InTech, 2011).
18. S.M. Sze and K. K. Ng, *Physics of Semiconductor Devices* (John Wiley & Sons Inc., 2007).
19. S. Cova, M. Ghioni, A. Lacaita, C. Samori and F. Zappa, "Avalanche photodiodes and quenching circuits for single-photon detection," Appl. Opt. **35**(12), 1956–1976 (1996).
20. B. Razavi, *Design of Integrated Circuits for Optical Communications* (McGraw-Hill Inc., 2003).
21. *Virtuoso Spectre, Product Version 14.1*, Cadence Design Systems Inc., San Jose, CA, USA (2014).
22. L.W. Snyman, M. du Plessis, and H. Aharoni, "Injection-Avalanche-Based n+pn Silicon Complementary MetalOxide Semiconductor Light-Emitting Device (450–750 nm) with 2-Order-of-Magnitude Increase in Light Emission Intensity," Jpn. J. Appl. Phys. **46**(4B), 2474–2480 (2007).
23. C. Favi and E. Charbon, "Techniques for fully integrated intra-/interchip optical communication," in *Proceedings of* 45th *ACM/IEEE Design Automation Conference* (2008), pp. 343–344.
24. A. Khanmohammadi, R. Enne, M. Hofbauer, and H. Zimmermann, "Monolithic Integrated Optical Random Pulse Generator in High Voltage CMOS Technology," in *Proceedings of 45th ESSDERC* (2015), pp. 138-141.
25. W. J. Kindt, "Geiger Mode Avalanche Photodiode Arrays," PhD dissertation (Delft University of Technology, 1999).
26. M. W. Fishburn, "Fundamentals of CMOS Single Photon Avalanche Diodes," Ph.D. dissertation (Delft University of Technology, 2012).
27. A. Rochas, "Single Photon Avalanche Diodes in CMOS Technology," Ph.D. dissertation (École Polytechnique Fédérale de Lausanne, 2003).
28. M. Sergio and E. Charbon, "An intra-chip electro-optical channel based on CMOS single photon detectors," in *IEEE International Electron Devices Meeting, 2005. IEDM Technical Digest.*, pp. 819–822.
29. M.J. Lee, P. Sun, and E. Charbon, "A first single-photon avalanche diode fabricated in standard SOI CMOS technology with a full characterization of the device," Opt. Express **23**(10), 13200–13209 (2015).
30. S. Radovanovic, A.J. Annema, and B. Nauta, "A 3 Gb/s optical detector in standard CMOS for 850 nm optical communication," IEEE J. Solid-State Circuits **40**(8), 1706–1717 (2005).

1. Introduction

Many smart power applications require data communication with galvanic isolation. Currently this is achieved using inductive isolators (transformers), capacitive isolators or discrete opto-couplers [1]. Integrated transformers are big and significantly add to cost and size while they are also prone to external electro-magnetic interference (EMI) [1]. Capacitive isolators can be integrated in the backend, but are relatively big when isolating between voltage domains that have a large voltage difference. Optocouplers are immune to EMI effects and monolithic integration of optocouplers is attractive for smart power and on chip communication applications [2].

Wide spectrum electroluminescence (EL) from silicon (Si) p-n junctions operating in avalanche mode has been reported earlier [3–5]. Avalanche mode light emitting diodes (AMLEDs) are fast with reported small signal modulation speed in the range of tens of GHz [6]. An AMLED as a light source in a CMOS integrated optocoupler has also been proposed [5, 7–10]. The coupling efficiency between the AMLED and an Si PD has been reported to be higher as compared to the same LED in forward mode of operation [10, 11]. This is because of the stronger overlap between the emission spectrum of Si AMLEDs and the spectral responsivity of Si PDs [7].

For optocoupling applications with a sufficiently low bit error rate (BER), the AMLED driver must ensure a certain minimum number of photons at the receiver side for data communication. However, optoelectronic properties of AMLEDs are sensitive to process, voltage and temperature (PVT) variations [12]. Together with their steep current-voltage (IV) curve at relatively high voltages, this easily results in high power consumption, and significant heating [10, 11] which

are bottlenecks to implement power efficient On-Off Keying (OOK) LED driver circuits in optocoupling applications. In this work, we introduce an AMLED driver circuit to solve these issues, enabling low power Si integrated optical transmitters.

Section 2 of this paper describes several physics related properties of the AMLED that are relevant for this work. We present an estimate of the transmission efficiency of our designed optical link in section 3 which is essential to characterize the AMLED in terms of its photon flux output. The principle of the driver circuit is to drive the AMLED (per data bit) with a minimum quantity of avalanche charge required to get certain amount of detectable photons at the PD, independent of PVT variations. The circuit to implement these features is introduced in section 4. The robustness, low power consumption and emission properties of the AMLED integrated with the driver circuit are demonstrated using the measurement results in section 5. Section 6 discusses the potential of using the AMLED with the introduced driver circuit in a monolithically integrated CMOS optocoupler. We conclude our work in section 7.

2. Optoelectronic properties of the AMLED

Figure 1(a) shows a schematic cross section of an AMLED (not to scale) in a 140 nm SOI CMOS technology [13]. The Medium Trench Isolation (MTI) regions and Buried Oxide (BOX) layer isolate the high voltage at the AMLED from the CMOS circuitry and provide galvanic isolation from the receiver. Figure 1(b) shows the TCAD simulated 2-D electric field profile (in the y-z plane), for the regions in the dashed box in Fig. 1(a). The field was simulated above breakdown: at a reverse bias (V_{BIAS}) of 18 V having a breakdown voltage (V_{BR}) of the AMLED of ~ 17 V. Avalanche breakdown and hence avalanche mode light emission is initiated in the region with the highest electric field [14], indicated in Fig. 1(b). Further, light is emitted mainly from the n^+ periphery that is closest to the p^+ contact (along x-axis) in Fig. 1(b). Figures 1(c)-1(d) show the TCAD simulated electron and the hole current density for the dashed region in Fig. 1(a).

A schematic top view of the AMLED and the integrated PD, including their dimensions is shown in Fig. 2(a). Two identical diodes have been used, one acting as an AMLED and the other acting as a PD. Hence the schematic cross section of the PD is same as shown in Fig. 1(a). Figure 2(b) shows the micrograph of the AMLED and PD. This PD is used only to measure photon flux of the AMLED as discussed in section 5.2. Figure 2(c) shows an EL-micrograph of the AMLED demonstrating emission at one side (along the x-axis indicated in Fig. 2(a)) as explained by our TCAD simulation results in Fig. 1(b)-1(d). Figure 2(d) shows the emission spectrum of the AMLED as measured vertically. Fabry-perot interference in the back-end causes the ripples in this vertical emission spectrum.

Measured reverse IV characteristics of the AMLED are shown in Fig. 3(a); for circuit simulations, these characteristics were used in a table-based (interpolated) IV model combined with a junction capacitance model. V_{BR} is defined as the voltage at which the I_{AMLED} starts to sharply increase. Figure 3(b) shows a linear relation between the AMLED avalanche charge (Q_{AMLED}) and the vertically emitted number of photons as calculated by Eq. (2) (section 3). For Fig. 3(b), the AMLED was biased at several DC currents (I_{AMLED}) using an Agilent B2901A source and measurement unit (SMU) (with measurement integration time = 1 s) and the vertical emission spectrum was measured using an Avantes ADC-1000-USB spectrometer with measurement integration time ($T_{\mathrm{integration}}$) of 30 s at each setting. Q_{AMLED} is calculated as $Q_{\mathrm{AMLED}} = \int_0^{T_{\mathrm{integration}}} I_{\mathrm{AMLED}}(t)\mathrm{d}t$.

3. Optical link transmission efficiency, η_{TE}

From a system level perspective, the total number of photons received at the PD per bit ($N_{\mathrm{photons,PD}}$) in response to the electrical energy spent in the AMLED per bit (E_{b}) is important. As discussed in section 5.2, E_{b} is proportional to the number of electrons flowing through

Optics EXPRESS

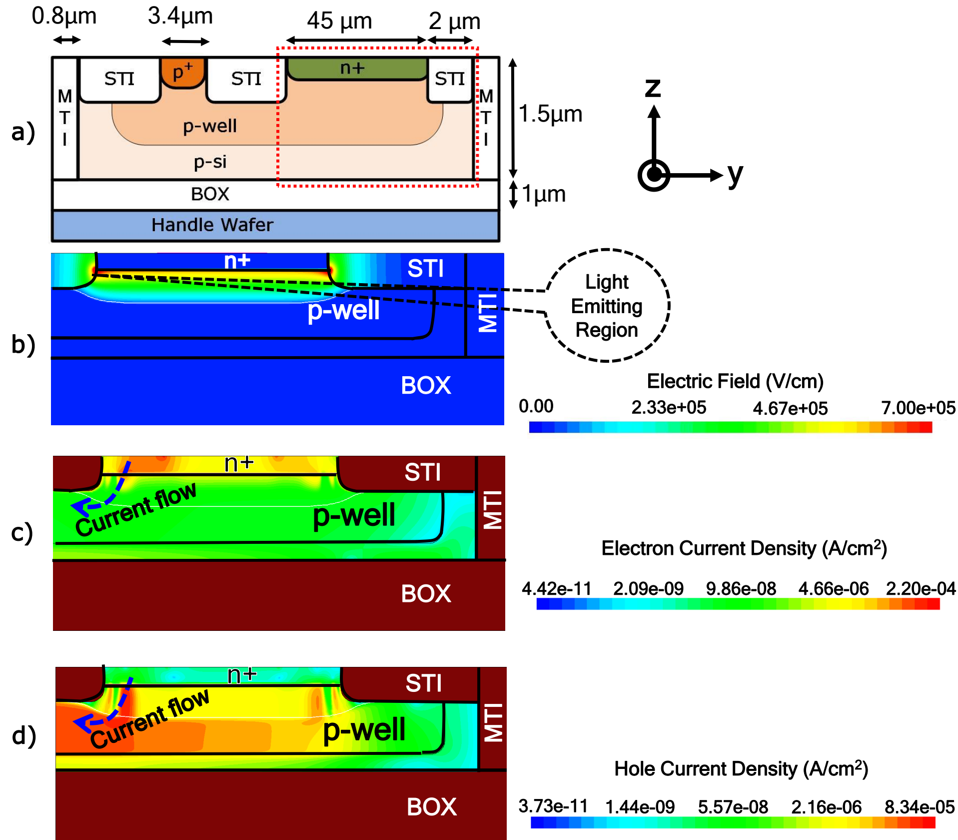

Fig. 1. (a) A schematic cross section of the n^+-pwell AMLED (not to scale). For the PD, the same device structure with equal dimensions has been used. (b) TCAD simulated electric field of the highlighted region in Fig. 1(a) at $V_{\mathrm{BIAS}} = 18$ V: Light is emitted from the indicated region. (c) TCAD simulated electron current density. (d) TCAD simulated hole current density.

the AMLED per bit ($N_{\mathrm{electrons,AMLED}}$). For estimating $N_{\mathrm{photons,PD}}$ in response to $N_{\mathrm{electrons,AMLED}}$, the total coupling quantum efficiency of the link (η_{system}) should be determined; we define η_{system} as $\eta_{\mathrm{system}} = \frac{N_{\mathrm{photons,PD}}}{N_{\mathrm{electrons,AMLED}}} \propto \frac{N_{\mathrm{photons,PD}}}{E_{\mathrm{b}}}$. This η_{system} can be written as the product of two efficiencies. The first one is the internal quantum efficiency (IQE) of the AMLED which relates the number of photons emitted per bit from the AMLED ($N_{\mathrm{photons,AMLED}}$) to $N_{\mathrm{electrons,AMLED}}$ [15]. The second efficiency component is the transmission efficiency of the optical link between the AMLED and the PD, denoted as η_{TE}.

$$\eta_{\mathrm{system}} = IQE \cdot \eta_{\mathrm{TE}} = \frac{N_{\mathrm{photons,AMLED}}}{N_{\mathrm{electrons,AMLED}}} \cdot \frac{N_{\mathrm{photons,PD}}}{N_{\mathrm{photons,AMLED}}}. \quad (1)$$

The IQE is estimated from DC measurements in section 5.2. In this section, we estimate the η_{TE}. Figure 4 represents the schematic structure of our design. The following steps describe our η_{TE} estimation procedure:

1. The total number of photons emitted by the AMLED ($N_{\mathrm{photons,AMLED}}$) is calculated. As shown in Fig. 2(c), light emission occurs predominantly at the lower edge of the AMLED.

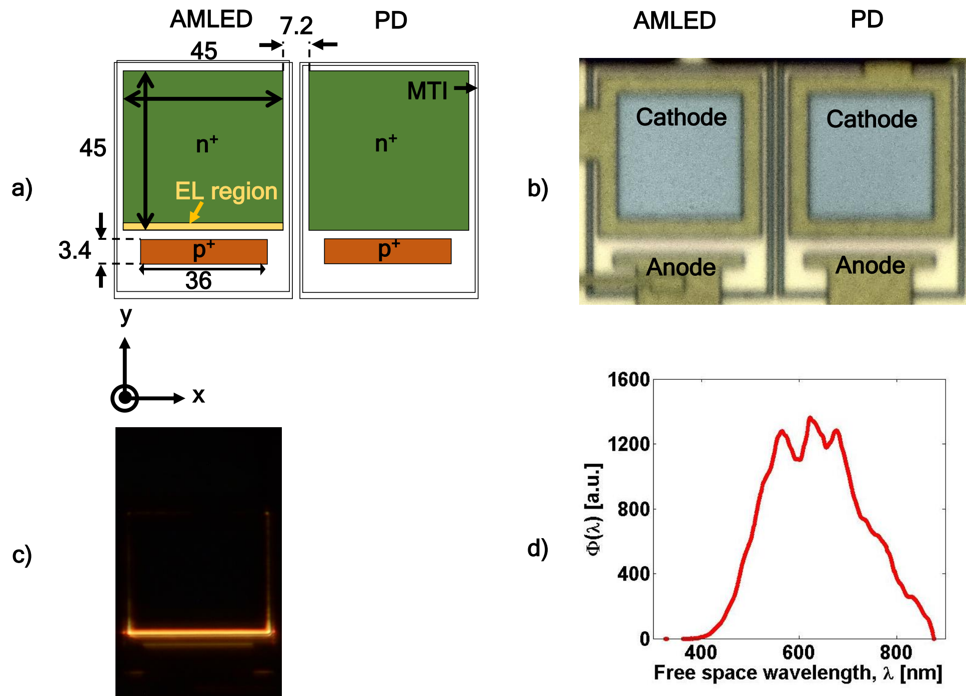

Fig. 2. (a) Schematic top view of the AMLED and the PD which are basically identical diodes; all dimensions are in μm. (b) Micrograph of the designed AMLED-PD structure. (c) Micrograph of the light emission from the AMLED using 25 s camera integration time, biased at a 4 mA DC current using an Agilent B2901A. (d) Emitted photon spectral flux density ($\Phi(\lambda)$) at 298 K ambient temperature; measured vertically using an Avantes ADC-1000-USB spectrometer and an integration time of 30 s. The arbitrary units [a.u.] are because of the unknown capture efficiency of the spectrometer.

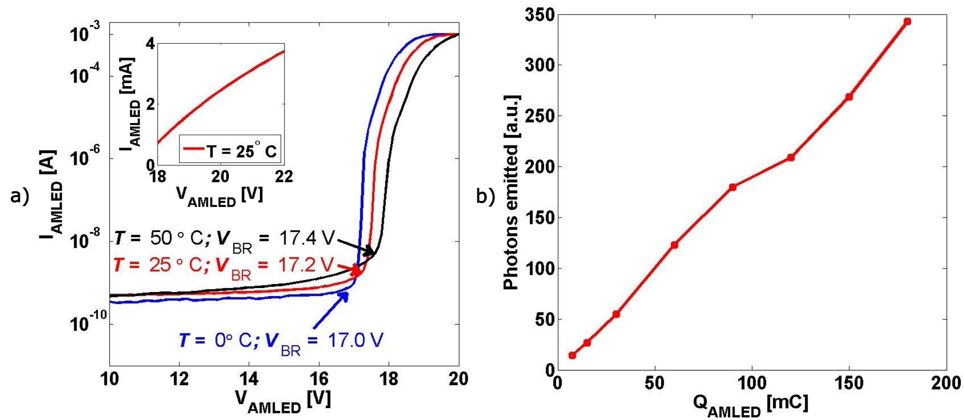

Fig. 3. (a) Measured AMLED reverse IV characteristics at several temperatures using an Agilent B2901A and with 1s integration time. The inset shows the IV characteristics (on linear scale) in the breakdown region to explicitly show the resistance (~ 1.45 kΩ) of the AMLED. (b) Estimated total number of vertically emitted photons (arbitrary units) as a function of AMLED charge (Q_{AMLED}).

Optics EXPRESS

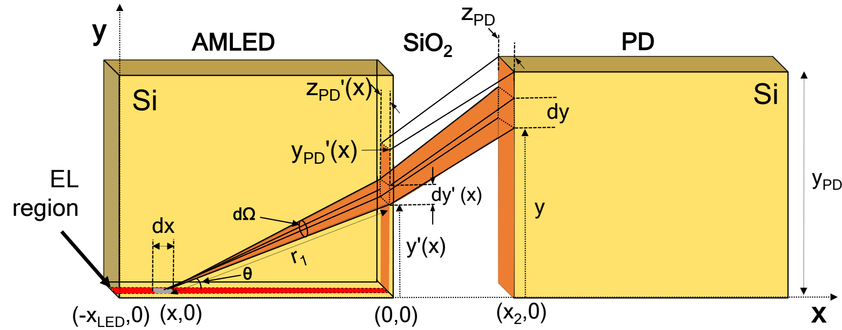

Fig. 4. Schematics of the AMLED-PD to estimate the optical transmission efficiency (η_{TE}). For the estimation, each light emitting point is assumed to emit isotropically. For clarity, important dimensions are enlarged. x_{LED} is the width of the AMLED (=45 µm), x_2 (= 7.2 µm) is the separation between the AMLED and the PD and z_{PD} = 1.5 µm is the thickness of the SOI layer.

We model this light emitting region as a line of length x_{LED}, of which each point is emitting uniformly and isotropically [16, 17]. Hence, some photons are emitted towards the top and bottom of the chip considering the isotropic nature of the emission. Photons emitted towards the top of the chip enable e.g. the micrograph of the light emission in Fig. 2(c) and $\Phi(\lambda)$ in Fig. 2(d). For simplicity reasons, any waveguiding effect through the BOX layer has been neglected. The total number of photons emitted by the AMLED ($N_{photons,AMLED}$) is given by:

$$N_{photons,AMLED} = \int_{\lambda} \Phi(\lambda)\, d\lambda, \tag{2}$$

where $\Phi(\lambda)$ is the photon spectral flux density, shown in Fig. 2(d).

2. The total number of photons received at the PD ($N_{photons,PD}$) is calculated; it is assumed that $N_{photons,PD}$ is limited only by [18]:

   - absorption losses in the AMLED. The absorption coefficient (α) is λ dependent and for this layout of the AMLED and the PD (as shown in Fig. 2(a)), most of the photons emitted at short λ are absorbed in the AMLED itself before reaching the PD.
   - the finite solid angle of the PD over the AMLED. The solid angle is limited either by the critical angle at the Si-SiO_2 interface or by the (apparent) size of the PD (Fig. 4). Due to refraction at the Si-SiO_2 interface, the apparent height of the PD seen at each point along the x-axis of the AMLED is different: the apparent height of the PD (y_{PD}) is reduced to $y'_{PD}(x)$. Similarly, the width of the PD (z_{PD}) is reduced to $z'_{PD}(x)$.
   - the transmittance at the Si-SiO_2 interfaces ($T_X(x, y)$), which is given by Fresnel's equations [15]. To simplify our calculations, constant (λ-invariant) refractive indices (n) have been used for Si (n =3.9) and SiO_2 (n =1.5).

   Along the x-direction, the lateral dimensions of the PD are much larger than the absorption length of the photons in the spectral region of interest. Therefore it is assumed that all the photons that reach the PD are detected.

   Along the z-direction, for the DC measurements (section 5.2), any photon absorbed within a diffusion length from the depletion edge of the PD will contribute to the photocurrent [18].

Optics EXPRESS

Under these assumptions and using Fig. 4, the received photon spectral flux density per unit length at the PD is:

$$\Phi_{PD}(x, y, \lambda) = \Phi_{LED}(\lambda) \cdot \exp\left(-\alpha(\lambda) \cdot r_1(x, y'(x))\right) \cdot T_X\left(0, y'(x)\right) \cdot T_X\left(x_2, y\right) \cdot \Omega(x, y), \quad (3)$$

where:

- $\Phi_{LED}(\lambda) = \frac{\Phi(\lambda)}{x_{LED}}$ is the emitted photon spectral density per unit length.
- $r_1(x, y'(x)) = \sqrt{x^2 + (y'(x))^2}$ is the distance traveled by photons emitted at $(x, 0)$ within the AMLED, while propagating towards (x_2, y).
- $T_X(0, y'(x))$ is the transmittance of the AMLED-SiO_2 interface and $T_X(x_2, y)$ is the transmittance of the SiO_2-PD interface.
- $\Omega(x, y) = \frac{d\Omega}{dy'} = \frac{z'_{PD}(x) \cdot cos(\theta)}{4\pi r_1^2(x, y'(x))}$ is the solid angle per unit length subtended by the PD over the dx section of the AMLED.

The total number of photons received at the PD because of emission from the entire light emitting area of the AMLED ($N_{photons,PD}$) is given by:

$$N_{photons,PD} = \int_0^{-x_{LED}} \int_0^{y'_{PD}(x)} \int_\lambda \Phi_{PD}(x, y, \lambda)\, d\lambda\, dy'\, dx. \quad (4)$$

3. Using numerical integration in Eq. (4), the $\eta_{TE} = (\frac{N_{photons,PD}}{N_{photons,AMLED}})$ of the link is estimated as 3×10^{-4}.

It is emphasized that the η_{TE} of this link is low due to mainly the sub-optimum (side-by-side) layout of the AMLED and the PD, as shown in Fig. 2(a) and 2(b). A possible direction to improve η_{TE} will be discussed in sec. 6.

4. AMLED driver circuit for an optocoupler

The main idea of the circuit is to drive the AMLED with a minimum amount of avalanche charge per data bit (Q_b), required to get a certain amount of photons at the PD, independent of PVT variations, with a relatively small area and relatively low demands on the driver circuit (including timing demands).

Figure 5 shows the principle of the self-quenched AMLED driver circuit (using idealized time domain waveforms) that limits the Q_b by dynamically quenching the avalanche process. We denote the voltage across the AMLED as $V_{AMLED}(= V_{BIAS} - V_{CAP})$. The excess bias voltage across the AMLED (V_{EX}) is defined as the extra voltage above V_{BR} [19], $V_{EX} = V_{AMLED} - V_{BR}$. The current through the AMLED is denoted as I_{AMLED} and the series resistance of the AMLED for $V_{AMLED} > V_{BR}$ as R_{AMLED}. $R_{AMLED}(\sim 1.45\ k\Omega)$ is estimated from the measured IV characteristics of Fig. 3(a) and is assumed constant for $V_{AMLED} > V_{BR}$ for simplicity [19]. The junction capacitance of the AMLED in and near avalanche is modeled by capacitance C_{AMLED}. The resistance of the driver circuit is negligible in comparison to R_{AMLED} and hence is ignored. A simplified model for the AMLED is also shown in Fig. 5 including the capacitance of the AMLED (C_{AMLED}) [19]. For this section, we assume $C_{AMLED} << C_Q$ for simplicity reasons.

We now describe the operating principle using Fig. 5. Initially, the voltage across the C_Q (V_{CAP} - V_{DRV}) is 0. First reset switch M1 is opened (using control signal RST) after which the input (IN) is set high at $t = 0$. As IN is set high, the V_{DRV} becomes low and instantly V_{CAP} also becomes low, the initial $V_{AMLED} = V_{BIAS} - V_{CAP} \approx V_{BIAS}$ and $V_{EX} = V_{BIAS} - V_{BR}$ (assuming $C_{AMLED} << C_Q$). The initial V_{EX} yields an initial $I_{AMLED} = V_{EX}\ /\ R_{AMLED}$.

Optics EXPRESS

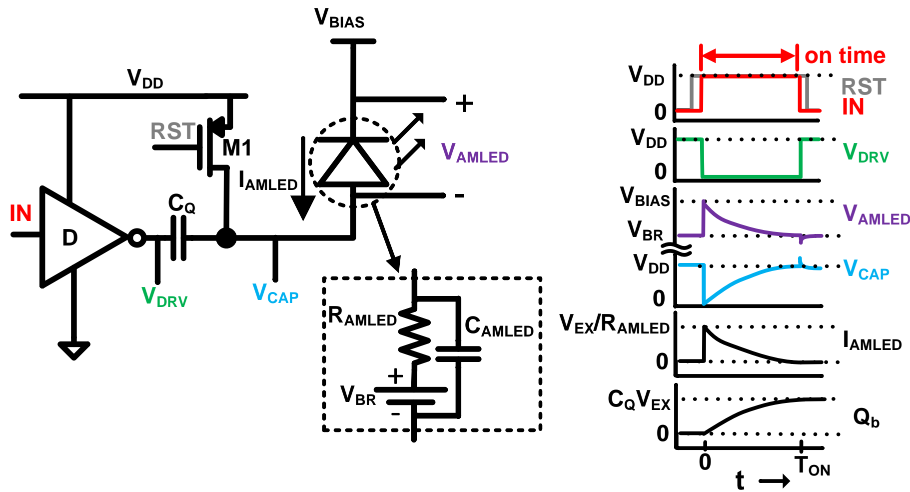

Fig. 5. Principle of the self-quenched driver circuit with idealized time domain waveforms. For our AMLEDs, $V_{BIAS} >> V_{DD}$. A simplified model for the AMLED is shown in the dashed area [19]. Important voltage and current waveforms are also shown on the right.

After the AMLED goes into the avalanche, $I_{AMLED}(t)$ charges the quenching capacitor C_Q which results in approximately an exponentially increasing V_{CAP}, hence in approximately an exponentially decreasing V_{AMLED} and V_{EX}. As V_{AMLED} approaches V_{BR}, the avalanche is quenched.

After the on time (T_{ON}), first IN is set low turning the driver off and then M1 is closed to reset the V_{CAP} to V_{DD}. Since the avalanche quenches itself by reducing V_{AMLED} to V_{BR}, we denote this circuit a self-quenched driver circuit.

$V_{AMLED}(t)$, $V_{EX}(t)$, $I_{AMLED}(t)$ and $Q_b(t)$ can be estimated: assuming the total resistance to be R_{AMLED} and the total capacitance to be C_Q, Equations (4) describe the mentioned physical quantities for $0 \le t \le T_{ON}$. The initial V_{EX} has been denoted as $V_{EX,0}$.

$$V_{AMLED}(t) = V_{BIAS} - V_{EX,0} \cdot \left(1 - \exp(-\frac{t}{R_{AMLED}C_Q})\right) \quad (5)$$

$$V_{EX}(t) = V_{EX,0} \cdot \exp(-\frac{t}{R_{AMLED}C_Q}) \quad (6)$$

$$I_{AMLED}(t) = \frac{V_{EX,0}}{R_{AMLED}} \cdot \exp(-\frac{t}{R_{AMLED}C_Q}) \quad (7)$$

$$Q_b = \int_0^{T_{ON}} I_{AMLED}(t)\mathrm{d}t = V_{EX,0}C_Q \cdot \left(1 - \exp(-\frac{T_{ON}}{R_{AMLED}C_Q})\right) \le C_Q V_{EX,0} \quad (8)$$

Equation (8) shows that Q_b is limited to $C_Q V_{EX,0}$ ($\le C_Q V_{DD}$).

The complete schematics of the implemented circuit are shown in Fig. 6(a). The driver circuit comprises of a chain of inverters (with enable functionality to switch C_Q) and a reset transistor. Selecting a C_Q value is achieved using a number of parallel identical drivers (D1 to D7) connected to the AMLED anode which can be controlled using their respective enable (EN) signals. Using D8 (identical to D1 to D7), the AMLED can be operated without any quenching (Fig. 10(c)-(d)). To enable the measurement of fast AMLED current transients at the onset of the avalanche, a differential structure is adopted and measurement circuit was implemented using an open drain PMOS differential amplifier [20]. The measurement setup enables us to measure at frequencies

Optics EXPRESS

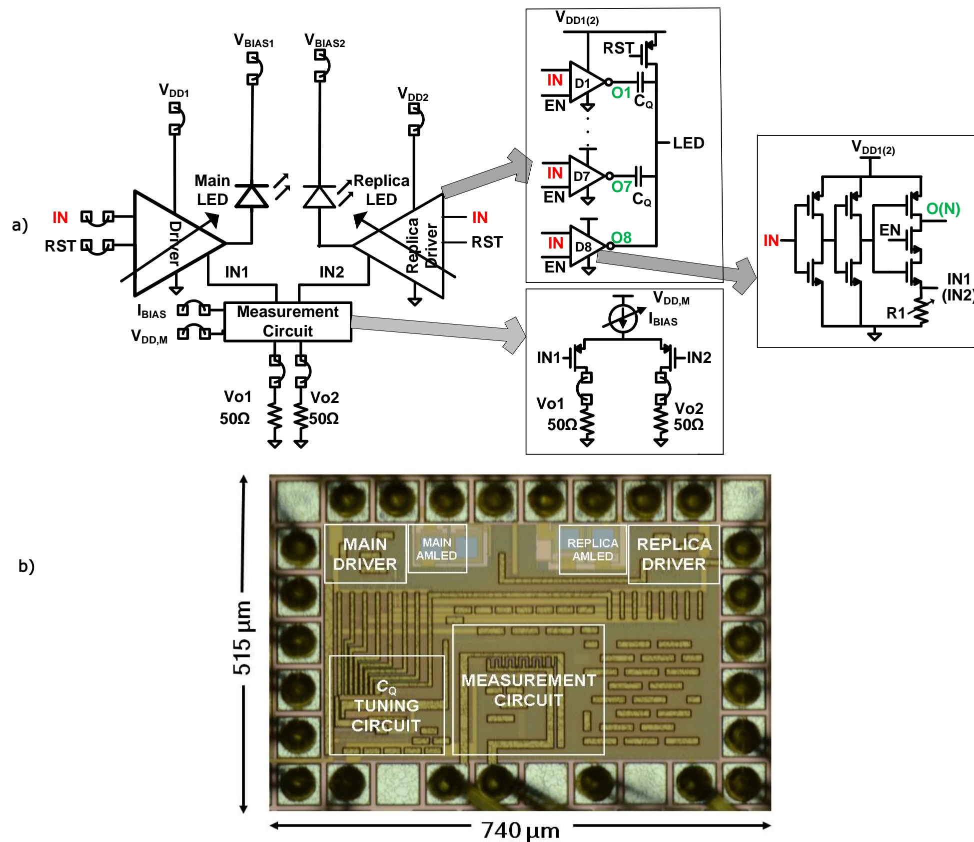

Fig. 6. (a) Complete schematics of the integrated AMLED driver and the measurement circuit. (b) Micrograph of the implemented chip. The chip was packaged without any top cover to measure vertical light emission from the AMLED. Also, no tiling was used over the AMLED area to avoid light blocking by the backend. Total area of the chip is 0.38 mm^2, the area of the main driver is 0.024 mm^2 and the area of the AMLED is 0.0033 mm^2.

upto 2.8 GHz. A micrograph of the implemented chip in a 140 nm CMOS SOI technology is shown in Fig. 6(b) [13]. We will show that this driver circuit is robust to many physics issues related to the power dissipation and PVT variations of an AMLED.

5. Measurement results

In this section, to demonstrate the functionality of the circuit, we show an example of the measured transient avalanche current (I_{AMLED}) waveform. Further, we show the measured energy-per-bit (E_{b}) of the presented transmitter and its photon flux output with respect to E_{b}. We also demonstrate the robustness of E_{b} against process, voltage, temperature, design and pulse width variations.

5.1. *Functionality*

With an off-state $V_{\mathrm{AMLED}} \approx V_{\mathrm{BR}}$, in the on-state the AMLED is driven to $V_{\mathrm{AMLED}} \approx V_{\mathrm{BR}} + V_{\mathrm{EX,0}}$ where $V_{\mathrm{EX,0}}$ is V_{DD} divided between C_{Q} and C_{AMLED} at $t = 0$ (using the simplified model of the

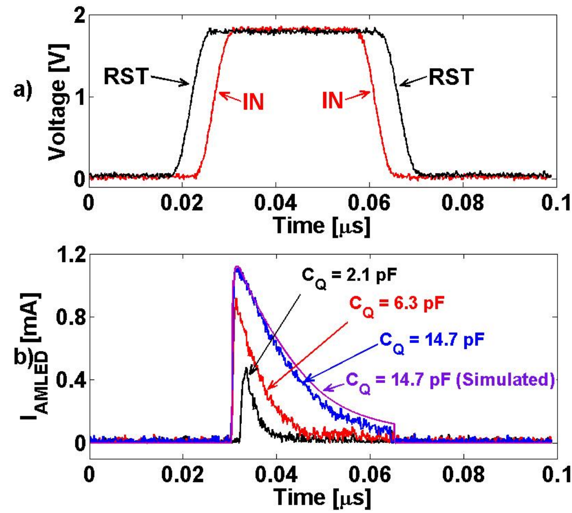

Fig. 7. (a) Control signals (IN and RST). (b) Measured transient waveforms of I_{AMLED} for three different C_{Q} settings at f_{s} = 10 Mbit/s. For clarity, only three settings are shown. Simulated transient data are also shown only for C_{Q} = 14.7 pF for clarity.

AMLED shown in Fig. 5).

$$V_{\mathrm{EX},0} = V_{\mathrm{DD}} \frac{C_{\mathrm{Q}}}{C_{\mathrm{Q}} + C_{\mathrm{AMLED}}} \tag{9}$$

Measured transient waveforms of I_{AMLED} at T_{ON} = 35 ns, pulse repetition rate (f_{s}) = 10 Mbit/s are shown in Fig. 7 for three different C_{Q} settings at V_{DD}=1.8 V. C_{AMLED} was measured to be about 650 fF at V_{AMLED} = 15 V (close to V_{BR}). For a lower C_{Q}, $V_{\mathrm{EX},0}$ is lower (Eq. (9)) and hence the magnitude of the I_{AMLED} (= $V_{\mathrm{EX},0}/R_{\mathrm{AMLED}}$) decreases (Fig. 3(a)). The charging rate of C_{Q} is limited by the R_{AMLED} (estimated as ~ 1.45 kΩ from Fig. 3(a)). Simulated transient data (using Spectre [21]) were obtained using a lookup table based model of the DC AMLED *IV* characteristics (Fig. 3(a)) in combination with a junction capacitance model for C_{AMLED} (Fig. 5).

5.2. Energy-per-bit and emitted photon flux per bit of the AMLED

From an electrical point of view E_{b} is a key Figure of Merit (FoM) [2]; E_{b} is defined as the energy required to transfer Q_{b} through the AMLED:

$$E_{\mathrm{b}} = V_{\mathrm{BIAS}} Q_{\mathrm{b}} \tag{10}$$

where V_{BIAS} is the DC bias voltage at the AMLED cathode (Fig. 6). E_{b} is limited by C_{Q} (Eq. (8), Eq. (9)):

$$E_{\mathrm{b}} = V_{\mathrm{BIAS}} Q_{\mathrm{b}} \le V_{\mathrm{BIAS}} C_{\mathrm{Q}} V_{\mathrm{EX},0} \le V_{\mathrm{BIAS}} C_{\mathrm{Q}} V_{\mathrm{DD}} \tag{11}$$

Fig. 8(a) shows an example of the measured E_{b} as a function of C_{Q}. The simulated E_{b} in Fig. 8(a) was obtained using Spectre [21], showing a good agreement with the measured E_{b}. The slight difference could be explained by the variations in C_{AMLED} with V_{AMLED}, which has been assumed constant in our simplified model (Fig. 5). The loss in the driver circuit was estimated to be about 21 pJ/bit.

For on-chip optical data communication, the lateral photon transmission to a nearby PD is relevant. To measure this, we integrated a calibration PD next to the AMLED (see Figs. 2(a)-2(b)).

Optics EXPRESS

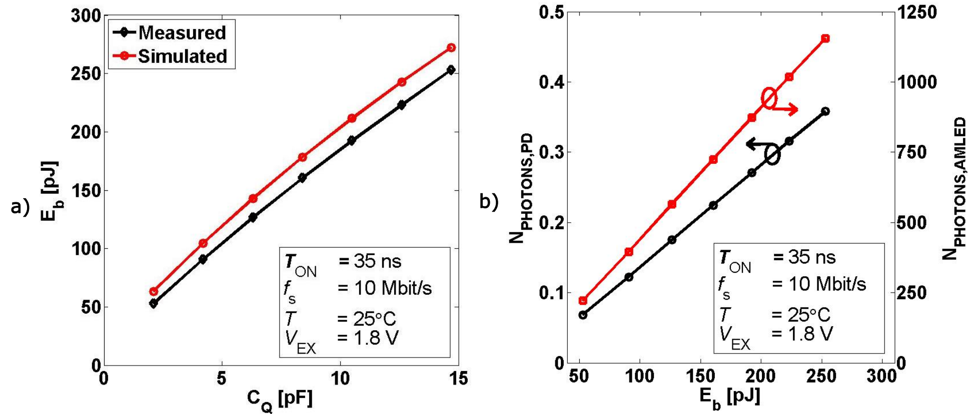

Fig. 8. (a) Measured and simulated E_b as a function of C_Q. (b) Estimated $N_{photons,PD}$ and $N_{photons,AMLED}$ as a function of E_b. $N_{photons,PD}$ and $N_{photons,AMLED}$ are photons per bit.

The AMLED is operated in OOK mode at f_s and the average PD photocurrent (I_{PD}) is measured. Using I_{PD} and f_s, the number of photons received at the PD per bit ($N_{photons,PD}$) can be estimated (Eq. (12)). We have assumed the quantum efficiency of the PD (η_{PD}) to be unity in the wavelength region of interest because the dimensions of the PD are much larger than the absorption length of the photons [18].

$$N_{photons,PD} = \frac{I_{PD}}{\eta_{PD} \cdot q_e \cdot f_s} \tag{12}$$

where q_e (= 1.6×10^{-19} C) is the elementary charge.

Figure 8(b) shows an example of the measured $N_{photons,PD}$ (on left y-axis) at different E_b settings at T_{ON} = 35 ns and f_s = 10 Mbit/s. It shows that $N_{photons,PD}$ depends linearly on E_b. Using $\eta_{TE} = 3 \times 10^{-4}$ (as derived in section 3 for our sub-optimum AMLED-PD layout) and $N_{photons,PD}$, the total number of photons emitted by the AMLED per bit ($N_{photons,AMLED}$) for different E_b settings can be estimated (Eq. (13)); an example of the estimated $N_{photons,AMLED}$ is also shown in Fig. 8(b) (on right y-axis).

$$N_{photons,AMLED} = \frac{N_{photons,PD}}{\eta_{TE}} \tag{13}$$

Like $N_{photons,PD}$, $N_{photons,AMLED}$ also depends linearly on E_b. Using $N_{photons,AMLED}$ and the number of electrons through the AMLED per bit ($N_{electrons,AMLED} = \frac{Q_b}{q_e} = \frac{E_b}{V_{BIAS} q_e}$), the internal quantum efficiency (IQE) of the AMLED (Eq. (1)) is estimated to be about 1.4×10^{-5}, comparable to what was also reported for Si earlier [22]. Using IQE and n_{TE} (section 3), the total coupling quantum efficiency of the link (η_{system}) is estimated as 4×10^{-9}.

As an estimation for continuous mode operation, we measured an I_{PD} = 8 pA at an I_{AMLED} =2 mA for the same optical link including identical diodes confirming the η_{system} as 4×10^{-9} for DC conditions [11].

Figure 9(a) shows the measured $\Phi(\lambda)$ of the vertical emission of the AMLED (along the z-axis in Fig. 4), driven at T_{ON} = 35 ns, f_s = 10 Mbit/s, for several values of C_Q, demonstrating that the $\Phi(\lambda)$ is almost proportional to C_Q, with a minor effect on the spectrum. Only four C_Q settings are shown for clarity. The increase in intensity with increasing C_Q is because of increasing Q_b.

Figure 9(b) shows the vertical photon flux density per bit, $\Phi_b = \frac{1}{f_s} \int_\lambda \Phi(\lambda) d\lambda$, as a function of E_b, demonstrating a linear relation between E_b and Φ_b.

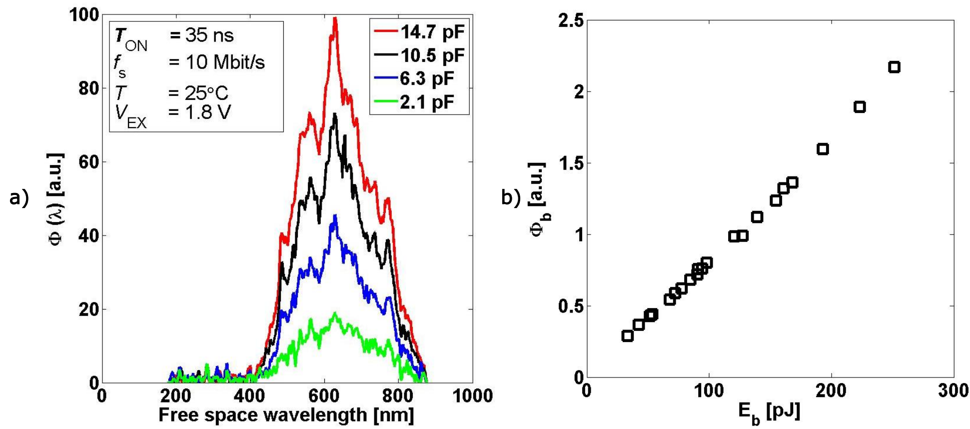

Fig. 9. (a) Measured vertical photon spectral flux density for several C_Q using an Avantes ADC-1000-USB spectrometer with an integration time of 30 s. (b) Measured vertical photon flux density per bit (Φ_b) as a function of E_b.

5.3. *Robustness of* E_b

We demonstrate the robustness of our circuit to process, voltage, temperature, design and pulse width (T_{ON}) variations using E_b as the FoM. Note that using the results shown in Fig. 8(b), E_b can be translated into $N_{photons,PD}$.

Figures 10(a)-10(b) show measured E_b as a function of C_Q across PVT and AMLED design variations, demonstrating that E_b is hardly affected by these variations but can properly be tuned by setting different C_Q values. For process variations, three different samples (D1, D2 and D3 from the same processing batch) were used. To explicitly show robustness of the proposed driver circuit with design variations, a number of n^+p diodes and a single p^+n diode were measured, driven by a replica driver circuit. E_b is non-linear with respect to C_Q because the pulse width (T_{ON}) is not sufficient to charge large C_Q completely (Eq. (8) and Fig. 5). For the p^+n AMLED, V_{BR} ≈14.4 V, $R_{AMLED} \approx 560\ \Omega$ and $C_{AMLED} \sim 585$ fF. A slight difference between the E_b of the n^+p AMLED and the p^+n AMLED is because of the different R_{AMLED}, C_{AMLED} and V_{BR}. The higher linearity in E_b with respect to C_Q in our p^+n AMLED is because of its low R_{AMLED}.

Figure 10(c) shows E_b for conventional (non-quenched) OOK drivers that show a large sensitivity to PVT variations and (especially) design variations. The measured E_b for the two AMLEDs are drastically different which is because of the different *IV* characteristics.

In data communication using OOK, the pulse width (T_{ON} in Fig. 5) is of importance. Figure 10(d) shows the impact of the pulse width (T_{ON}) on E_b: for the self-quenched driver the E_b is mainly determined by the selected C_Q, for pulse repetition rate (f_s) to ∼ 10 Mbit/s. At lower T_{ON}, the E_b drops due to mainly R_{AMLED} that determines the maximum Q_b and hence the E_b (Eq. (8), Eq. (11)).

For comparison, the non-quenched operation of the AMLED in Fig. 10(d) shows a strong T_{ON} (hence timing) dependency. The simulated E_b (using Spectre) shows a good agreement with the measured E_b. For the non-quenched driver circuit, E_b can be estimated as $E_b \approx V_{BIAS} I_{AMLED} T_{ON} = V_{BIAS}(V_{EX}/R_{AMLED}) T_{ON}$. Using the self-quenched circuit, E_b (thus power dissipation) is always lower than $C_Q V_{DD} V_{BIAS}$ independent of T_{ON} (Eq. (11)).

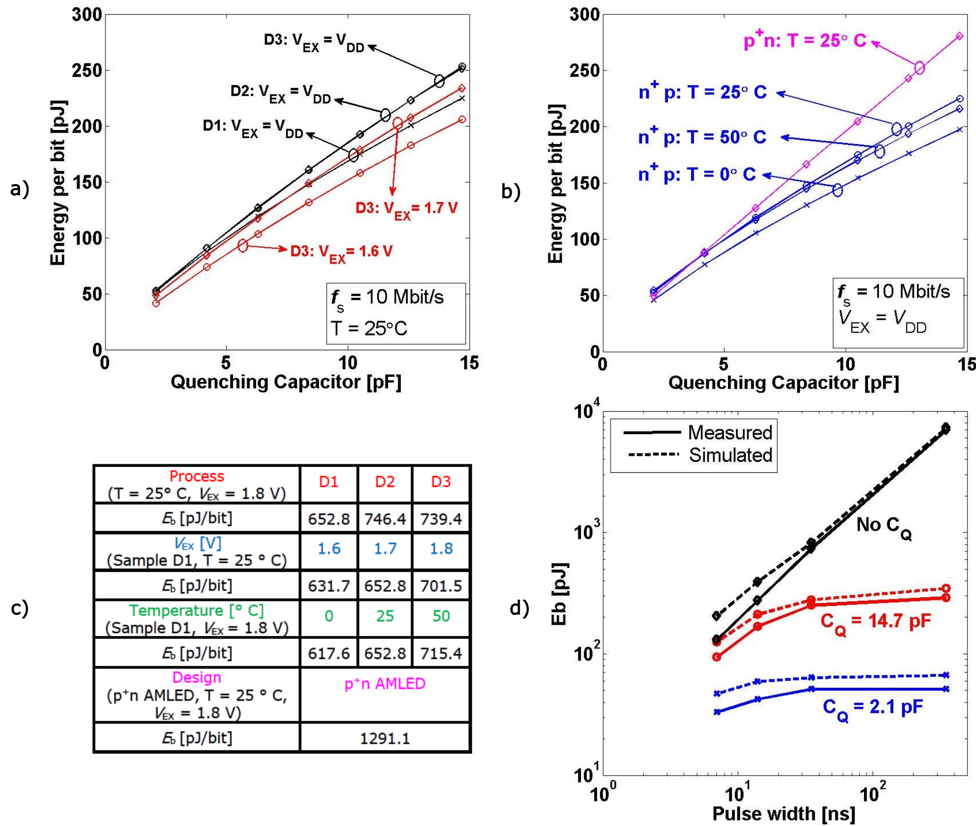

Process (T = 25° C, V_{EX} = 1.8 V)	D1	D2	D3
E_b [pJ/bit]	652.8	746.4	739.4
V_{EX} [V] (Sample D1, T = 25 ° C)	1.6	1.7	1.8
E_b [pJ/bit]	631.7	652.8	701.5
Temperature [° C] (Sample D1, V_{EX} = 1.8 V)	0	25	50
E_b [pJ/bit]	617.6	652.8	715.4
Design (p⁺n AMLED, T = 25 ° C, V_{EX} = 1.8 V)	p⁺n AMLED		
E_b [pJ/bit]	1291.1		

Fig. 10. Measured E_b of an AMLED driven by the self-quenched driver circuit compared to using a traditional non-quenched driver circuit. (a) The n^+p AMLED: process and voltage variations. (b) The n^+p AMLED: temperature variations and E_b vs C_Q for the p^+n AMLED. (c) E_b for non-quenched circuits for the n^+p and p^+n AMLED. (d) Effect of pulse width (T_{ON}) on E_b for the n^+p AMLED.

6. Application in opto-couplers

In this section, first we discuss the potential of the proposed optical transmitter for application in opto-couplers. In a further section, we discuss the aspects of the transmission bit rate.

6.1. Optocouplers in CMOS technology

Although our work mainly focused on the transmitter in a fully Si-integrated optical link, the demonstrated optical transmitter aims at applications in a complete optical link in Si. For the minimum E_b setting (~ 53 pJ/bit), the n^+p AMLED emits 220 photons per bit isotropically (Fig. 8(b)). Using Fig. 8 and the model presented in section 3, it is possible to optimize the optical link geometry to receive e.g. 5 photons at the PD out of $N_{photons,AMLED}$. To receive more than 5 photons out of 220, it is required that $\eta_{TE} > 2 \times 10^{-2}$. For instance, when the AMLED and the PD are aligned as shown in Fig. 11, the η_{TE} of the link is estimated to be 2×10^{-2} using the method in section 3. Further suggestions to improve η_{TE} such as patterning the link, improving the AMLED design have been extensively discussed in [11]. It is also beneficial to have optical transmission paths for such optical links for waveguiding the photons from the AMLED to the

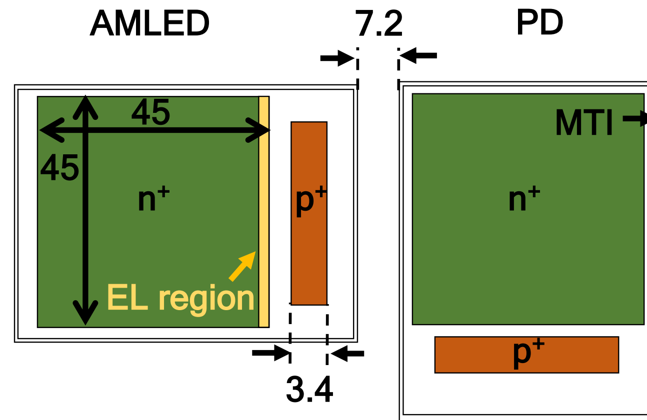

Fig. 11. Proposed layout of the AMLED and the PD to increase the η_{TE}.

PD. This will improve the coupling quantum efficiency, as well as reduces the crosstalk among multiple channels in a multi-channel communication environment.

If 5 photons are received at the PD per bit, this is typically sufficient to operate a well-designed Single Photon Avalanche Diode (SPAD) as a PD [19, 23–28]. SPADs are p-n junctions biased above V_{BR} so that an incoming photon in the depletion region can generate free carriers thus triggering an avalanche [25–27]. The macroscopic avalanche current can then be easily measured by using digital simple read out circuitry. The design of SPADs and SPAD read out circuits are well-known in CMOS technologies [25–27]. Recently, a SPAD designed in the same technology has been reported [29].

Further, in the current link geometry a large jitter would occur if 5 photons per bit were statistically received at the PD. This is because many free carriers are generated by the photons outside the depletion region which subsequently diffuse towards the depletion region triggering the SPAD after some ill determined diffusion time. Therefore, it is recommended to design links with a higher η_{TE} and to capture photons mainly in the depletion region. This could be achieved by using e.g., a lower doping in the PD which results in a wider depletion region [18]. This is a topic of future research.

6.2. *Transmission bit rate*

The transmission bit rate is ultimately limited by the speed of the detector (SPADs or the PDs). AMLEDs have been reported to have a very high modulation speed, in the range of tens of GHz [6].

For SPADs, the achievable bit rate is limited by their deadtime requirement. To reduce the unpredictable and hence undesired aferpulsing phenomena in SPADs, the deadtime of the SPADs after each photon counting event has to be increased, which limits the bit rate of the SPADs [26], [29]. For the SPADs that were reported in this technology [29], the bit rate would be limited to about 10 Mbit/s based on their reported deadtime (~ 100 ns). The major challenge would be improving SPAD designs to have a lower deadtime requirement.

Using conventional photodiodes, higher bit rates can be achieved, however at the cost of increased power consumption in the AMLED. This is because of its required continuous operation mode to increase the signal-to-noise ratio (thereby to reduce the bit error rate) at the PD. A data rate of 3 Gbit/s has been reported with an integrated Si receiver in a standard 180 nm CMOS

technology using off chip illumination [30].

Measurements of maximum achievable data rate using the proposed detectors is also a topic for future research.

7. Conclusion

In this work, a low power monolithically integrated optical transmitter using avalanche mode LEDs (AMLEDs) was designed in a standard 140 nm SOI CMOS technology. The novel self-quenched driver circuit resolves many physics issues related to power dissipation and PVT variations of an AMLED. This work successfully demonstrates a low power wide spectrum optical transmitter in CMOS technologies that can be integrated with standard Si detectors. It further reinforces the promise of enabling AMLEDs as light sources for Si CMOS technology for monolithic integration of optocouplers in CMOS [5, 10, 11, 22].

Funding

Dutch Technology Foundation (STW) (HTSM 2012, Project 12835).

Acknowledgments

The authors would like to thank NXP Semiconductors B.V. for fabricating the chip and Henk de Vries and Gerard Wienk (Integrated Circuit Design, University of Twente) for the technical and experimental support. The authors are also thankful to the esteemed reviewers for their constructive comments which have improved this paper, and the editor for arranging the review.

131.180.131.48 {ts '2017-09-20 09:41:41'}